Design and Performance of Insect Inspired High Frequency Flapping Wing Robots

Zheng Hu and Xinyan Deng, *Member, IEEE*

***Abstract*— A 2.61 gram high frequency flapping wing robotic insect actuated by DC motor with lift up to 47mN was developed. The design features a passive rotation mechanism and can incorporate both artificial and real insect wings. Wing beat frequency is up to 65Hz and the lift production increases with the wing beat frequency. Experiments were carried out to verify the reconfigurable flapping amplitudes regarding the design of crank rocker transmission. Results show that 120° amplitude is the optimal configuration for lift to power efficiency. Both manmade wings and cicada wings were compared in lift generation. Near field and far field flow measurements using particle image velocimetry system show clearly the flow velocity and vorticity around the wing such as the leading edge vortex, induced flow, and tip vortex. The comparative study using man-made and cicada wings showed more uniform flow and lift force coefficients on cicada wings.**

I. Introduction

The recent surge of interest in the development of micro aerial vehicles capable of hovering and fast maneuvering has led to several efforts to develop flapping wing robotic devices inspired by insects or birds[1-7]. From the physical viewpoint, it is clear that the aerodynamic mechanisms underlying flapping flight differ in many fundamental ways from those governing fixed wing flight [8-10]. The key advantages that flapping flight offers over fixed wings is the ability to hover and the possibility of generating stable flight forces through a high angle of attack motion without appreciable stall. This enables sustained, high lift force over greater duration thus making them attractive alternatives to traditional fixed wing devices. Meanwhile, the key advantages that flapping flight offers over rotorcraft such as a micro-helicopter are their superior flight performance such as maneuverability, stability, and robustness under external disturbances such as wind gusts. Indeed, it appears that diverse biological systems have exploited these basic advantages of flapping wings to ensure superior aerodynamic performance (Birds[11], Bats [12], Insects [8, 13], Ptreopods [14], Seeds[15]).

Inspired by the aerobatic performance of birds and insects and taking cue from the developments in flapping wing aerodynamics (for reviews see [8, 10, 16, 17]), several engineering groups have been developing flapping wing flying robots [1-7, 18, 19]. For example, the Berkeley Micromechanical Flying Insect (MFI) project, the Harvard robotic insect lab, and the CMU Nanorobotics lab have all developed life-size 60-mg Piezo-actuated micromechanical fly capable of lifting its own weight [3, 6, 20]; the recently developed 10-gram hummingbird inspired Nano Air Vehicle (NAV) by Aerovironment has demonstrated successful hovering and forward flight controlled through a remote controller[21]; the Delfly which were able to perform autonomous flight and navigation through complicated environment with an on-board camera [5], to name just a few. The challenges on robotic insect development include flapping mechanism design, high frequency requirement, hovering capability, and most importantly lift generation. In recent years, few groups have demonstrated lift generation that exceed the body weight of their insect-inspired robots[2, 22]. However, detailed investigation of flow structure around the insect robot, both near and far field, is still very limited. As aerodynamic performance and lift generation depends critically on the wing and mechanisms design, such information is crucial in the design, optimization, and diagnosis of flapping wing mechanisms.

In this study, we present the design of DC motor driven robotic insect prototypes and measure their aerodynamic performance. To this end, we have developed several generations of bio-inspired robotic insect wing mechanisms including high frequency flapping wing mechanisms with one-paired or double-paired wings, for example, life-size cicada-inspired robots and dragonfly-inspired four-winged robots. The latest generation of a 2.61-gram cicada robot is able to generate 4 grams of lift and achieve up to 65Hz wingbeat frequency under the inputs of less than 12 Volts. For this study, we systematically measured the lift generation and flow structures around these robots, by varying the wingbeat frequency and wing materials including manmade wings and real cicada wings. Wing kinematics were measured using high speed camera. Lift to power ratio was also systematically measured for various flapping amplitudes. Near and far field flow measurements were performed under hovering configuration in a wind tunnel using digital particle image velocimetry system. These measurements are the critical first steps to aid the wing design and optimization of such MAV devices with desired aerodynamic performance.

II. Robot Design

A. Overall design

An overview and photo of such insect-size flapping robots developed in the Bio-robotics Lab of Purdue University are shown in Fig.1. It employs horizontal stroke plane similar to most of Dipteral insects. The wing has two degrees of freedom - flapping and ration. The reciprocating wing strokes are realized through a gear-crank-rocker mechanism; meanwhile a passive wing rotation mechanism was employed

This work was supported by NSF Grant 0545931 to X Deng. The School of Mechanical Engineering, Purdue University, West Lafayette, IN 47906. Email: xdeng@purdue.edu

so that the pronation and supination of wings result from the inertia and aerodynamics forces during the wing reversal. Mechanical stoppers were employed at the stroke reversal to constrain the maximum allowable rotation angles. The angle of attack (AOA) for both upstroke and downstroke is around 45º. The wing stroke angle amplitude are re-configurable and can vary among 100 º, 110 º, 120 º or 130 º; a frequency up to 65Hz was achieved at 12V power supply and under 100º amplitude configuration; the wing tip to tip distance is 114mm. The robot has height of 28mm and a total weight of 2.61 gram (excluding the power supply). The weight of a man-made wing is 0.04 gram with wing length of 46mm. Table I lists the main components of the robot and its weight distribution.

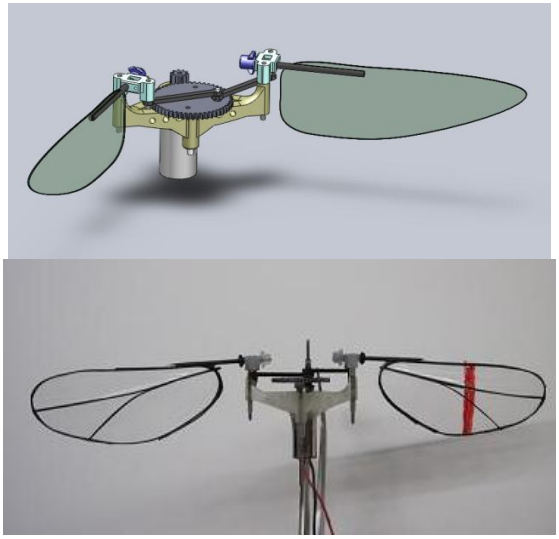

Fig. 1. CAD model and photo of the robotic insect.

Main parts	Material	Quantity	Weight (g)
Frame	FullCure 720	1	0.38
Gear & pinion	Delrin	2	0.23
Linkage	Carbon fibre	2	0.11
Wing house	FullCure 720	2	0.14
Wing stopper	FullCure 720	2	0.06
Wing	Carbon & Mylar	2	0.08
Pins & shafts	Stainless steel	8	0.32
Motor	MK-06	1	1.29
TOTAL			2.61

Table I. Robot parts list and weight distribution

B. Gear and crank-rocker transmission

The power from motor is transmitted to wings through a gear- crank-rocker mechanism which is a combination of gear transmission and crank-rocker transmission, shown in Figure 2 and 3. The gear ratio is set to be 5.2:1 for the gear drive. There are two symmetric for-bar sets for the two wings which share the same crank but equipped with their own four bar linkages.

The parameters for crank-rocker mechanism are shown in Fig. 3 and Table II. The ground link L0 and coupler link L2 are both 12mm; the rocker L3 is 5mm. The crank appears as parts of the driven gear. In order to achieve difference flapping amplitudes, four difference lengths can be configured for crank L1, shown in Table II. The flapping amplitude is considered as a critical design parameter regarding the efficiency on dynamics and aerodynamics, which will be tested and discussed in Section III.

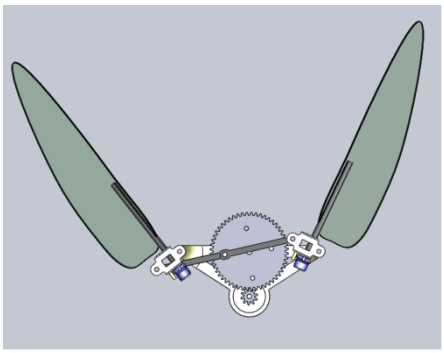

Fig. 2. Top view of power train

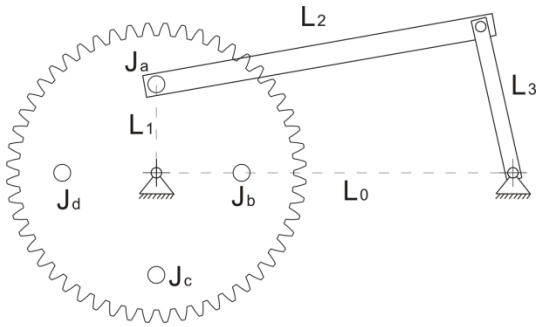

Fig. 3. Four bar mechanism analysis

Joint	L1 (mm)	Amplitude (°)	Press. Angle (°)
Ja	3.83	100	58.3
Jb	4.10	110	62.4
Jc	4.31	120	66.3
Jd	4.53	130	70.6

Table II. Configurations of cranks

C. Passive rotation mechanism

In order to achieve high frequency and high mechanical efficiency, we embedded a passive rotation feature into the design. It is highly compact and easy for assembly and disassembly. Fig.4 and Fig. 5 describe the mechanism in detail. The wing shaft rotates freely in the wing house (clearance fit), but is constrained in the axial direction with a collar made from Teflon tube (press fit). The end of wing shaft is connected to a wing stopper (purple) using coniform press fit, which highly simplifies the structure. Two sector skirts are designed on the stopper and a pin

(golden) is positioned on the wing house so that the rotation of stopper is constrained due to the meeting of pin and skirts. The size of vacancy between the two sectors determines the amplitude of passive rotation. In general the stoppers have been designed to achieve a 45° Angle of Attack (AoA), which was found to be aerodynamically optimal in insect flight [9].

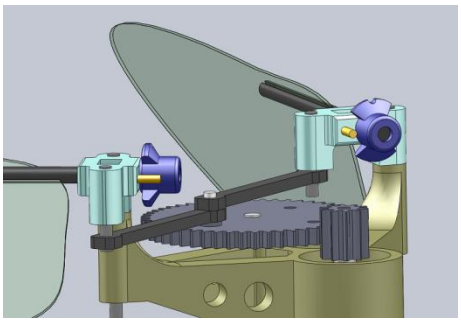

Fig. 4. Close-up view on passive rotation mechanism

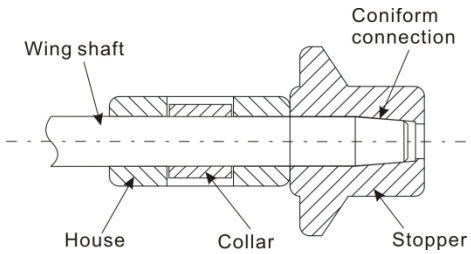

Fig. 5. Sectional view on passive rotation mechanism

D. Wings

Both cicada wings and manmade wings were incorporated into the design. Manmade wings were made from Mylar film (2um thickness) and carbon fiber strands. A carbon rod serves as wing root shaft. The weight is 0.04g for a single manmade wing while only 0.02g for a cicada wing. The trailing edge of cicada wing is much more flexible than manmade wing whose trailing edge rigidity comes from the glued carbon fiber strands.

Fig. 6. Samples of cicada wing and manmade wing

E. Lift force measurement platform

We designed an angular lever platform to measure the mean lift force (Fig. 7). A lever was setup on to a pivot and can rotate in the vertical plane about the pivot axis. The robot insect was fixed onto the left end of the lever with a distance of L to the pivot; a standard weight m_0 was put on the right part of the lever and its position was adjusted to make the combination (robot, lever and m_0) fully balanced, which means that it is balanced at any angular position for the lever, which also means the mass center of the combined system is on the pivot axis. This is critical for the accuracy of the measuring system.

A proper weight m was attached on the left side of lever with a distance of a to the pivot. When the robot flaps at a certain frequency and equation (1) is satisfied, the lever can recover the balance at a particular angular position θ' after several swings:

$$mga > LF_l \tag{1}$$

Considering both the pre-balance and the new balance, the lift force generated at this moment can be calculated by:

$$F_L = \frac{mga\cos\theta'}{L} \tag{2}$$

This lever platform can also be used to measure the side force generated by a single wing. For that purpose the MAV with a single wing should be rotated by 90 ° so that the wing is pointing downward.

Although the pivot generates negligible torque, the wire connection between the actuator and the DC power supply may have some undefined force transferred to the lever therefore cause measurement errors. We used two solutions to minimize this effect: 1) use thin copper wire of 0.13mm diameter (gauge 36) with max current of 500mA, since the actuator absorbs current no larger than 400mA; 2) Attach the wire to the lever from the pivot point to eliminate the torque generation from the wires.

To check the accuracy of the measuring system, we put a small mass on the position close to the robot under the pre-balance condition, and found that a mass of 0.02 gram is able to break the balance. Thus the sensitivity of the system is up to 0.02 gram. Considering the robot can generate lift forces above 1 gram, the system error is less than 2%.

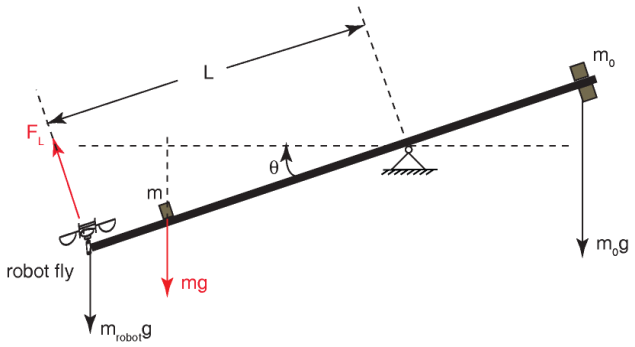

Fig. 7. The Angular Lever Platform

F. *Flow measurements using DPIV system*

To measure the flow on the high frequency flapping wings in air, we used a stereo Digital Particle Velocimetry (DPIV) system manufactured by TSI Inc. We used a dual-cavity pulsed YAG laser (120-mJ) at 532 nm wavelength to illuminate a flow field sheet of 1mm thickness. The air was seeded with submicrometre-sized particles of olive oil vapor, generated by a Laskin nozzle. Particle illumination was recorded with a pair of PowerView Plus 2MP, 1.6K x 1.2K pixel resolution, high Quantum Efficiency, low noise Digital CCD cameras equipped with 50mm/F1.8 camera lens. Data were processed by Insight 3G Image Capture, Analysis, and Display Software Platform built on Net technology with parallel processing capability and integrated TecPlot data presentation. We designed and built a phase lock circuit with a laser pointer and an optical sensor for phase averaged PIV measurements. The circuit will send a TTL pulse to the Synchronizer each time the wing passes the beam of laser pointer and triggers the laser and camera systems.

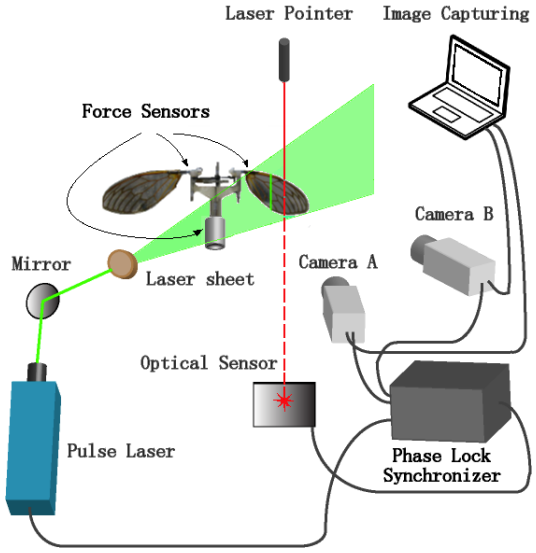

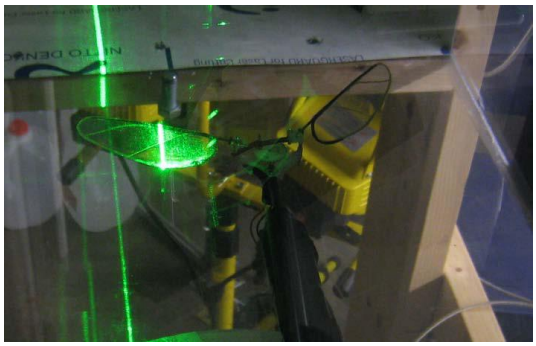

Fig. 8 Upper: The DPIV system setup for flow velocity and vorticity measurements: Lower: Position of the laser sheet with respect to the wing configured for near field flow measurements in the wind tunnel. The camera is to the left of the wind tunnel.

Both the frontal view (far field) and side view (near field) PIV test are carried out. In the side view PIV test, laser sheet intersected the wing at positions of 55%, 65%, 75% wing length from wingbase and are considered as the most significant lift generation area along the wing. In the frontal view, the camera is parallel to the wingspan and captures the downwash flow and vorticity of the induced flow.

III. Experimental Results

A. *Wing kinematics*

Slowed-down motion images of wings were captured by high speed cameras (Phantom 7) and the kinematics was derived from the camera images. Fig. 9 shows 8 sequences from the top view on one wing at 120º amplitude with wingbeat frequency of 40Hz. We derived the instantaneous flapping angle and rotational angle by calculating the leading edge position and the projection of a marked line on the wing. The results are shown in Fig.10. Due to the passive rotation design, there is a lag (about 6% of cycle) between stroke ending and wing flipping (angle of attack reversal).

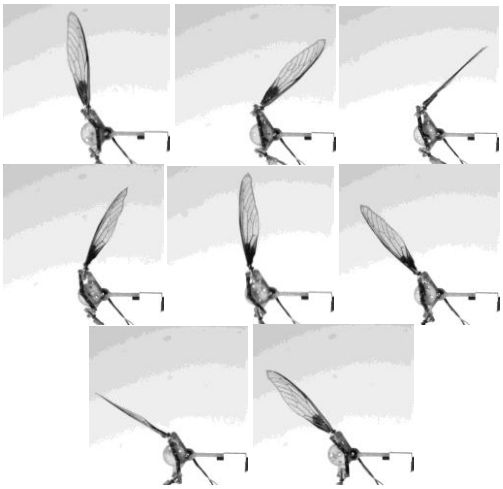

Fig. 9. A set of sequences of camera top view on cicada wing

The flapping amplitude configuration does not change the overall pattern of the flapping angle, but alters the duration of 'high AoA'. Here we define 'high AoA' as any angle of attack above 40º. Fig. 11 shows that the duration of high AoA increases as the flapping amplitude increases. As a result, the high lift duration is extended too, which may yield higher efficiency on lift production.

B. *Lift force measurements*

The mean lift forces are measured as input voltages vary from 3.5V to 8.5V. Meanwhile flapping frequency was measured using a tachometer. The results showed that flapping frequency increases almost linearly with the input voltage. The frequency of 42 Hz (in the figure) was recorded at 9V, and the highest frequency measured on the robot (with the same man-made wings) was 65Hz, operating at 12V input. However, significant buckling and deformation of the wing were observed beyond frequency of 45Hz on man-made wings and their efficiency also drops considerably.

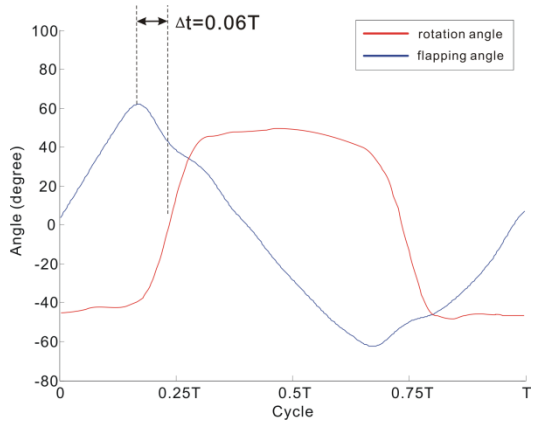

Fig. 10. Kinematics measurements at 120 º amplitude, 40Hz.

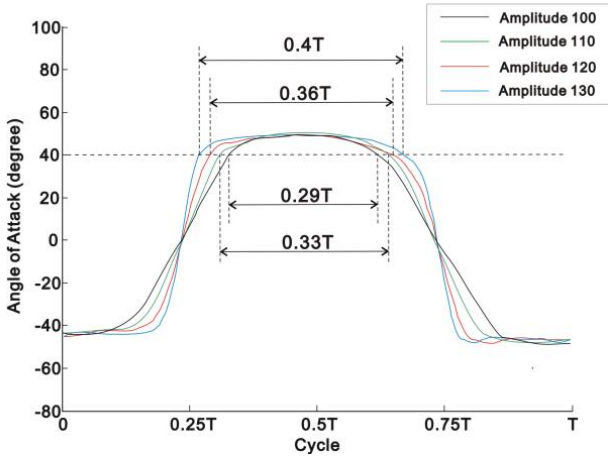

Fig. 11. Trace of AoA under different amplitude configurations.

The mean lift forces generated by the two types of wings - manmade and cicada wings - are shown in Fig. 12. The results show that in general, the lift force increases with frequency in a quadratic manner. However, as the frequency increases beyond 35Hz, the lift from manmade wing saturates, while the lift on cicada wings continues to increase. The 35Hz might be an upper limit for this particular set of manmade wings to keep the leading edge vortex (LEV) stable.

In particular, the cicada wings showed a good performance of lift force as well as the efficiency when 7.5 V was supplied. The lift force at this moment is 35.2 mN, which is large enough to support the weight of the body.

The lift coefficient was calculated according to the following equation:

$$C_L = \frac{F_L}{\rho R^3 \bar{c} \hat{r}_2^2(S) \left| \overline{\frac{d\phi}{dt}} \right|^2} \quad (3)$$

where ρ is the air density, R is wing length (48mm), $\bar{c}$ is mean chord length (13mm), $\hat{r}_2^2(S)$ (0.36) is the non-dimensional second moment of wing area, F_L is measured lift (for a wing pair), $\left| \overline{d\phi/dt} \right|$ is the mean wing angular velocity, which is approximated by $2\Phi n$, where Φ is flapping amplitude and n is flapping frequency. Fig. 13 shows the lift coefficient at different flapping frequency, the mean lift coefficient is at 1.91. For the tested frequency which ranges from 18 to 40Hz, the Reynolds number (3400 to 7500) is also close to the one of hawk moth (Manduca Sexta) flight. Assuming the body weight at 1.5 gram, a hawk moth need to achieve a mean lift coefficient at about 2.5 in order to hover, which is higher than the one measured in the current experiment. This might reflect some wing morphological and kinematical difference between the hawk moth and the robotic insect. Specifically, hawk moth flap asymmetrically for up and down strokes with a tilted stroke plane, and the robotic insect robot flaps horizontally. And hawk moth wings generally have wing twist and flexibility which could enhance the lift production at high angle of attack. Therefore, this result suggests that more careful design of wing flexibility and shape as well as kinematics could very likely increase the lift production.

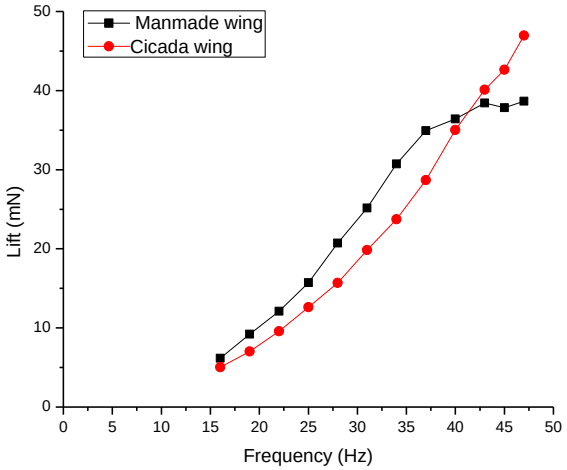

Fig.12. Mean lift force measured at different flapping frequencies.

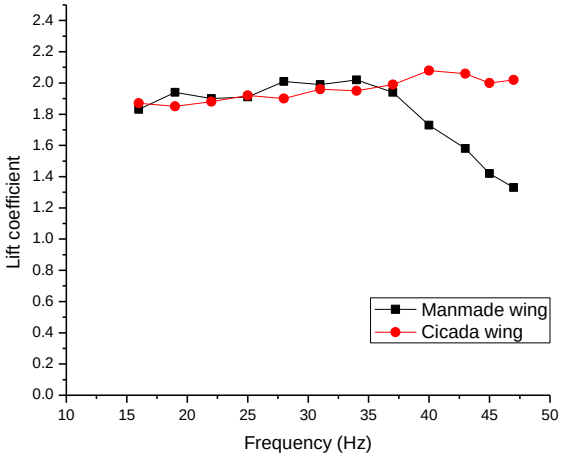

Fig.13. Lift coefficients at different flapping frequencies.

C. *Lift to power ratio*

Here we studied the lift to power ratios at the four amplitude configurations, as shown in Fig. 14. We conclude from Fig. 14 that, as expected and due to the extended 'high AoA', the lift to power ratio increases when amplitude increases from 100º to 120º, but starts to drop when increase further to 130º. One of the reason for the reduction is that the higher amplitude brings high pressure angle to the four bar transmission which generates a high load on the motor so that the electro-mechanical system becomes less efficient.

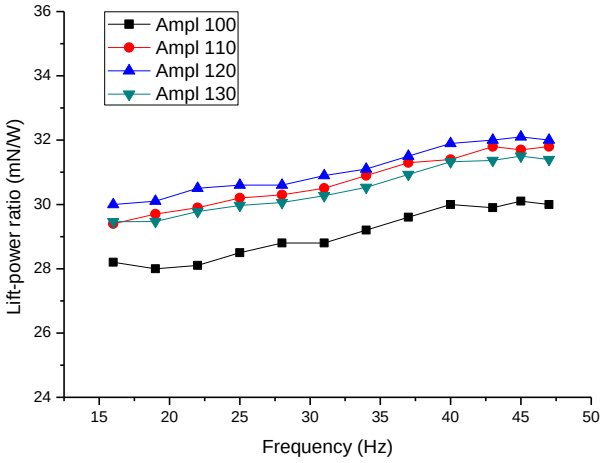

Fig. 14. Lift-power ratio under different amplitude configurations.

For each configuration, the lift to power ratio also increases slightly as the frequency goes higher. The ratio then reaches maximum at around 45 Hz. The frequency modulation is likely to be highly depended on resonant frequency of the wing. The common frequency for cicada is around 41Hz, which is around the resonant frequency of cicada wing.

D. *Near and far field flow measurements*

Flow measurements – both near and far field – are essential in investigation of the aerodynamic performance of life-size insect inspired wings. The dynamic evolution of vorticity and velicity fields, together with wing kinematics and force measurements, can inform a robot designer to choose or fabricate certain wing features for high aerodynamic performance. Figure 15 and 17 show the DPIV setup for measuring either near or far field flow vorticity and velocity fields. Figure 16 and 18 shows sample results on a man-made wing. As seen from Fig. 16 where the white line represents the wing chord and white dot represent leading edge of the wing, both leading edge vortex (LEV) and trailing edge vortex (TEV) are clearly present during midstroke. The LEV is well attached on the leading edge and is found to be the main mechanism responsible for lift generation on flapping wings[8]. Fig. 18 shows the vorticity and velocity of the induced flow (far field flow) during mid-downstroke, where the tip vortex and notch vortex are clearly shown.

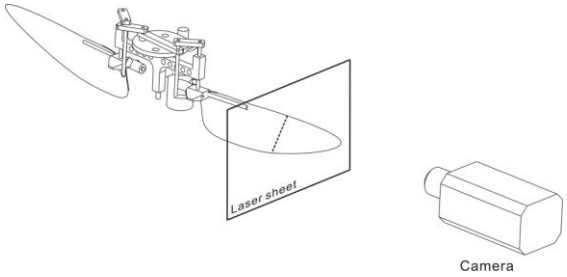

Fig. 15. Setup to investigate near field flow such as leading edge vortex (LEV).

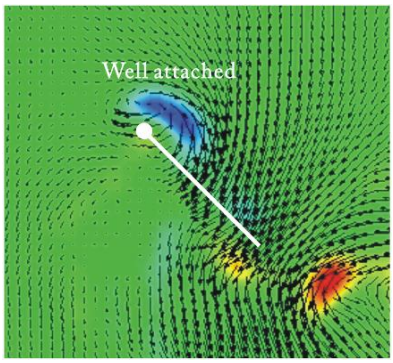

Fig. 16. Near field flow velocity and vorticity measured on 65% wing chord. Leading edge vortex (blue) and Trailing edge vortex (red) are clearly shown.

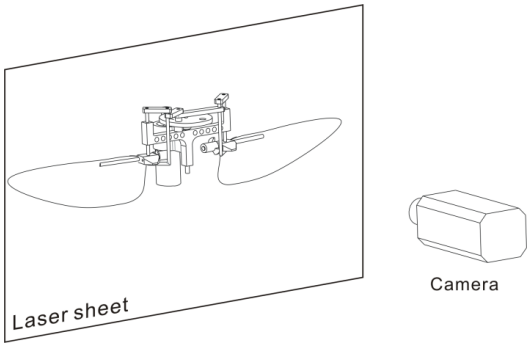

Fig. 17. Setup to investigate far field flow such as induced flow.

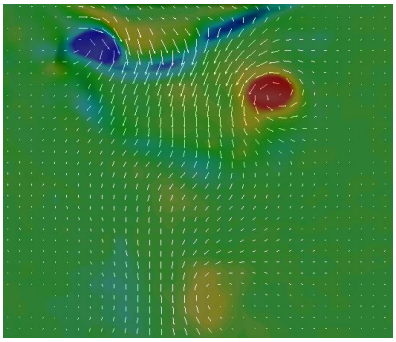

Fig. 18. Far field flow velocity and vorticity measured on one wing. Tip vortex (red) and notch vortex (red) are clearly shown.

E. Comparison of manmade and cicada wings

In order to explore the underlying reason for the lift saturation as the frequency goes above 35Hz in manmade wings, we carried out PIV experiments to visualize the vortex and induced flow patterns at different frequencies and compared them with those from the cicada wing. The LEV was examined from the side view PIV at 3 spanwise positions with a distance of 55%, 65% and 75% wing length from wingbase which are considered as the most significant lift generation area along the wing. The wake right below the wings was also studied in the frontal view PIV with a laser plane passing the middle of wing stroke. The results revealed two major findings on man-made wings: first, the LEV became more unstable and detached from leading edge at high frequencies; second, the downwash under the flapping wings diverged sideward in the frontal view at high frequencies.

Figure 19 shows the LEV on a manmade wing operating at around 45Hz. While the LEV firmly attaches to the leading edge of the wing with little shedding at 30Hz (Figure 16), when wings flap at 45Hz, the manmade wings buckle during flapping (from high speed camera images), and LEV lost its stability during the early stroke and starts to shed. On the other hand, the cicada wing still has a smooth wing motion with negligible buckling (from camera images), and the leading edge vortex is still firmly attached (Figure 20).

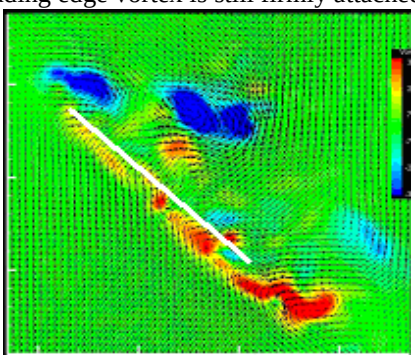

Figure 19. LEV and its detachment from the leading edge on manmade wing at 45Hz.

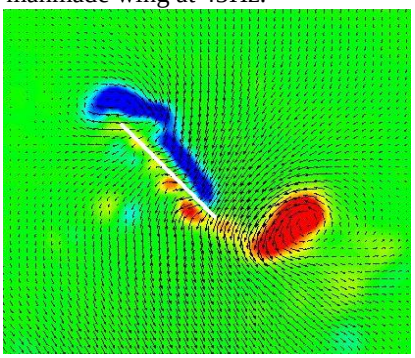

Figure 20. LEV and its attachment on the leading edge on cicada wing at 45Hz.

Previous experimental and computational studies have shown that lift force can be enhanced as LEV keeps attaching to the wing, while lift production suffer a significant as LEV sheds from the wing. Apparently in this case of particular man-made wing, this is a detrimental situation that should be avoided in MAV design. On the other hand, nature's solution with a real cicada wing (even when it's dry and brittle) still outperforms our current manmade wing design.

Furthermore, as we can see from Fig. 21, both downwash show a diverging pattern at a higher frequency (42Hz) on manmade wing. In fact at lower frequency (30Hz) the induced flow still pointed vertically downward. As flapping frequency gets higher, the induced flow starts to diverge sideways. Such a kind of divergence of downwash indicates that there is a considerable horizontal momentum put into fluid. Theoretically, the lift production on the wings is proportionate to the downward momentum put into the fluid, while the horizontal momentum only accounts for side forces. Therefore, as the frequency goes higher, the side force of MAV increases dramatically, while the lift tends to be saturated, as we seen in the force measurement results.

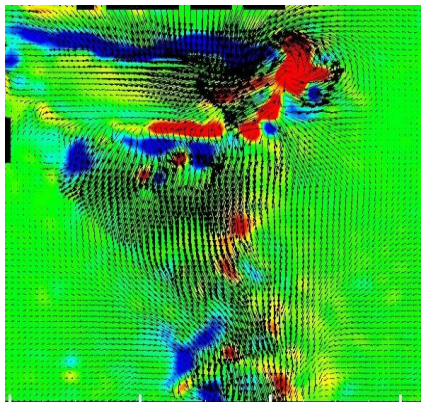

Figure 20. The downwash streamline pattern of manmade wing at 42 Hz. The induced flow shows diverging trend.

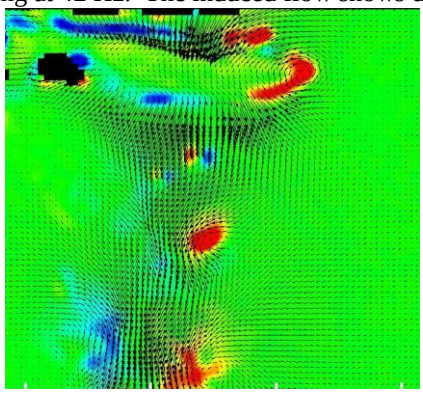

Figure 21. The downwash streamline pattern of cicada wing at 45 Hz. The induced flow is still pointing downward.

Meanwhile, in the front view PIV results (Fig. 22) of cicada wings, the downwash still keeps vertical (like those at lower frequencies) even if the flapping frequency goes up to 45Hz. Also, the tip vortices in this case are not as strong as those in manmade wing, thus the induced flow will be less driven sideways in the cicada wing. This configuration is considered to be efficient for lift production since on energy is wasted into horizontal momentum.

IV. Conclusions

In this paper, we present the detailed design of a high frequency robotic insect mechanism driven by DC motor with wingbeat frequencies up to 65Hz under 12V input. The wings are driven by a crank rocker mechanism for large amplitude flapping angles and angle of attack from passive rotation with mechanical stoppers. Experimental results on lift to power ratio show that high flapping amplitude brings high pressure angle in the power train and the electromechanical system becomes less efficient; while on the kinematics aspect, low flapping amplitude reduces the duration of high AoA which decreases efficiency on lift production. For the current design, 120º amplitude is found to the best for lift efficiency. Both manmade wings and cicada wings were compared in lift test and result show that the lift from manmade wings saturated with frequency beyond 35Hz, while lift on cicada wings was a continuous increase. Near field and far field flow measurements of both wings were investigated using a DPIV system. Results show that in the manmade wing the Leading Edge Vortex lost its stability and partially shed away when frequency increase beyond 35Hz. Furthermore, the induced flow generated on manmade wing diverges at high frequency, probably due to the strong tip vortices that were shed into the downwash. In the future, seeking solutions to minimize the wake divergence and stabilize LEV could be significant in order to promote the lift production on the MAV.

References

[1] X. Deng, Schenato, L., Sastry, S., "Flapping Flight for Biomimmetic Robotic Insects. I. System Modeling," *IEEE transaction on robotics*, vol. 22, pp. 776-788, 2006.

[2] E. Steltz, S. Avadhanula, and R. S. Fearing, "High Lift Force with 275 Hz Wing Beat in MFI," in *IEEE Int. Conf. on Intelligent Robots and Systems* San Diego, CA, 2007, pp. 3987-3992.

[3] R. J. Wood, "The First Takeoff of a Biologically Inspired At-Scale Robotic Insect," *Robotics, IEEE Transactions on*, vol. 24, pp. 341-347, 2008.

[4] R. J. Wood, S. Avadhanula, R. Sahai, E. Steltz, and R. S. Fearing, "Microrobot design using fiber reinforced composites," *Journal of Mechanical Design*, vol. 130, pp. -, May 2008.

[5] G. d. Croon, K. d. Clerq, R. Ruijsink, B. Remes, and C. d. Wagter, "Design, aerodynamics, and vision-based control of the DelFly," *International Journal of Micro Air Vehicles*, vol. 1, pp. 71-97, 2009.

[6] R. J. Wood, R. S. Fearing, "Flight Force Measurements for a Micromechanical Flying Insect," in *IEEE/RSJ International Conference on Intelligent Robots and Systems*, Maui, HI, 2001, pp. 335-362.

[7] V. A. Lindsey L. Hines, and Metin Sitti, "Control Performance Simulation in the Design of a Flapping Wing Micro Aerial Vehicle," in *2010 IEEE/RSJ International Conference on Intelligent Robots and Systems*, Taipei, Taiwan, 2010, pp. 1090-1095.

[8] M. H. Dickinson, F. O. Lehmann, and S. P. Sane, "Wing rotation and the aerodynamic basis of insect flight," *Science*, vol. 284, pp. 1954-60, Jun 18 1999.

[9] S. P. Sane and M. H. Dickinson, "The aerodynamic effects of wing rotation and a revised quasi-steady model of flapping flight," *J Exp Biol*, vol. 205, pp. 1087-96, Apr 2002.

[10] Z. J. Wang, "Dissecting insect flight," *Annu. Rev. Fluid Mech.*, vol. 37, pp. 183-210, 2005.

[11] B. W. Tobalske, T. L. Hedrick, K. P. Dial, and A. A. Biewener, "Comparative power curves in bird flight," *Nature*, vol. 421, pp. 363-6, Jan 23 2003.

[12] F. T. Muijres, L. C. Johansson, R. Barfield, M. Wolf, G. R. Spedding, and A. Hedenstrom, "Leading-edge vortex improves lift in slow-flying bats," *Science*, vol. 319, pp. 1250-1253, Feb 29 2008.

[13] C. P. Ellington, "The Aerodynamics of Hovering Insect Flight. IV. Aeorodynamic Mechanisms," *Philosophical Transactions of the Royal Society of London.*, vol. 305, p. 34, Feb.24 1984 1984.

[14] B. J. Borrell, J. A. Goldbogen, and R. Dudley, "Aquatic wing flapping at low Reynolds numbers: swimming kinematics of the Antarctic pteropod, Clione antarctica," *J Exp Biol*, vol. 208, pp. 2939-49, Aug 2005.

[15] D. Lentink, W. B. Dickson, J. L. van Leeuwen, and M. H. Dickinson, "Leading-Edge Vortices Elevate Lift of Autorotating Plant Seeds," *Science*, vol. 324, pp. 1438-1440, Jun 12 2009.

[16] F. O. Lehmann, "When wings touch wakes: understanding locomotor force control by wake wing interference in insect wings," *J Exp Biol*, vol. 211, pp. 224-33, Jan 2008.

[17] S. P. Sane, "The aerodynamics of insect flight," *J Exp Biol*, vol. 206, pp. 4191-208, Dec 2003.

[18] M. W. Oppenheimer, D. B. Doman, and D. O. Sigthorsson, "Dynamics and Control of a Biomimetic Vehicle Using Biased Wingbeat Forcing Functions," *Journal of Guidance Control and Dynamics*, vol. 34, pp. 204-217, Jan-Feb 2011.

[19] D. B. Doman, M. W. Oppenheimer, and D. O. Sigthorsson, "Wingbeat Shape Modulation for Flapping-Wing Micro-Air-Vehicle Control During Hover," *Journal of Guidance Control and Dynamics*, vol. 33, pp. 724-739, May-Jun 2010.

[20] L. Hines, V. Arabagi, and M. Sitti, "Free Flight Simulations and Pitch and Roll Control Experiments of a Sub-gram Flapping-Flight Micro Aerial Vehicle," in *IEEE International Conference of Robotics and Automation*, Shanghai, China, 2011.

[21] Aerovironment, "Hummingbird Nano Air Vehicle," http://www.avinc.com/uas/adc/nano/, 2011.

[22] R. Wood, "The first takeoff of a biologically-inspired at-scale robotic insect," *IEEE transaction on robotics*, vol. 24, pp. 341-347, 2008.